frontiers | Frontiers in Materials

TYPE Original Research
PUBLISHED 10 August 2022
DOI 10.3389/fmats.2022.941311

OPEN ACCESS

EDITED BY
Hasan Uludag,
University of Alberta,

REVIEWED BY
Ying Zhao,
Shenzhen Institutes of Advanced Technology, (CAS),
Fatemeh Kabirian,
Faculty of Medicine, KU Leuven,

*CORRESPONDENCE
Hai Kuang,
kuanghai@hotmail.com
Bo Li,
bli24@cmu.edu.cn

SPECIALTY SECTION
This article was submitted to Biomaterials, a section of the journal Frontiers in Materials

RECEIVED 11 May 2022
ACCEPTED 27 June 2022
PUBLISHED 10 August 2022

CITATION
Yan J, Huang W, Kuang H, Wang Q and Li B (2022), The effect of etched 3D printed Cu-bearing titanium alloy on the polarization of macrophage. *Front. Mater.* 9:941311. doi: 10.3389/fmats.2022.941311

The effect of etched 3D printed Cu-bearing titanium alloy on the polarization of macrophage

Jinge Yan[1], Wanyi Huang[1], Hai Kuang[2]*, Qiang Wang[1] and Bo Li[1]*

[1]School and Hospital of Stomatology, China Medical University, Liaoning Provincial Key Laboratory of Oral Disease, Shenyang, China, [2]Department of Oral and Maxillofacial Surgery, College of Stomatology, Guangxi Medical University, Nanning, China

3D printed titanium alloys have been widely used as implants in orthopedic surgery and dentistry. In recent years, Cu-bearing titanium alloys have shown great advantages in tissue engineering due to their excellent antibacterial activity and biological effect. In the current study, three alloys, namely, TC4 alloy, TC4-5Cu alloy, and TC4-6Cu alloy were fabricated by the use of selective laser melting (SLM) technology. Acid etching treatment was used to remove the metal powders on the samples and modify the surface of the manufactured alloys. The effect of different etched alloys on the biological behavior of macrophages (RAW 264.7) was studied comprehensively. Results showed that acid etching had no effect on the hydrophilicity, while contributing to the adhesion and polarization of macrophages with a lower ROS level. Moreover, Cu-bearing titanium exhibited better cell adhesion, macrophage polarization potential, and a lower ROS level. In summary, acid etching treatment provided a promising strategy to improve the biological properties of the Cu-bearing titanium alloys by SLM.

KEYWORDS

3D printing, copper, Ti6Al4V, acid etching, macrophage, ROS, oxidative stress

1 Introduction

As a common disease of oral surgery, maxillofacial bone defect caused by tumors, trauma, and other reasons affects the patients' appearance and directly harms the swallowing, chewing, and conversing functions of patients. In recent years, there have been two main approaches to repairing maxillofacial bone defects: surgical reconstruction and bone tissue engineering. However, surgical reconstruction has relative limitations in clinical application. Hence, bone tissue engineering plays an important role in maxillofacial bone repair. As one of the general bone tissue engineering technologies, 3D printing technology has been widely used in clinical practice in recent years due to its excellent characteristics, such as the ability to achieve personalized precise designs, be produced quickly and efficiently, and reduce the time and risk of surgical exposure (Dawood et al., 2015).

3D printing, also called additive manufacturing (AM), is a quick advanced technology that creates solid models by adding powder layer by layer. This technology has already been used for maxillofacial bone defects, dental defects, and dentition defects (Javaid and Haleem, 2019). The commonly used biomaterials are metals, alloys, ceramics, and polymers. These materials are used in different medical disciplines according to the requirements of specific applications. Previous research illustrated that metal materials were the most commonly used materials in dentistry due to their excellent mechanical properties (strength, hardness, wear resistance, durability, toughness, etc.) compared with ceramic materials and resin materials (Palaskar et al., 2010). Clinicians in the field of dentistry and orthopedic surgery demand materials with good mechanical properties, corrosion resistance, and biocompatibility, and titanium alloys largely meet these requirements.

In recent years, different metal elements are added to titanium alloys to improve the properties of the alloys. As one of the necessary micro-elements for the body, copper is a cofactor of various enzymes involved in the life activities of the body. In addition, copper is also widely used in various biomaterial research studies due to its excellent antimicrobial activity and biological activity (Zhang et al., 2016). Carter et al. (Carter et al., 2017) have verified that copper-bearing implants can inhibit the activity of both Gram-positive and Gram-negative bacteria. Huang et al. (Huang et al., 2019) demonstrated that copper-containing titanium alloy has good biocompatibility, and copper ions released from its surfaces could act as an inflammatory regulator to promote osteogenesis and sterilization.

A retrospective study on failed dental implants by Sun et al. (Sun et al., 2017) showed that 47% of early implant failures were caused by inflammation. Peri-implant diseases and infections have become the focus of oral implantology prevention and treatment (Spriano et al., 2018). Research studies have proven that compared with stainless steel materials (Chen et al., 2015) and poly-ether-ether-ketone (PEEK) (Olivares-Navarrete et al., 2015), titanium and titanium alloys have a lower level of inflammation and less abundance of macrophages on the surfaces. The implant-related inflammatory response can be summarized in the following eight steps: exudation, protein surface adsorption, growth of a temporary provisional matrix based on blood, the capacity of cells of the innate immune system to proliferate (white blood cells, platelets, complement, and blood coagulation system), neutrophil migration, by replacing the differentiation of the mononuclear cell into macrophages, foreign body reaction, generation of reactive oxygen species, and monocyte/macrophage fusion to form foreign body giant cells or apoptosis. Among them, reactive oxygen species production is an important step in the process of inflammatory response.

Reactive oxygen species (ROS) are cooperative or independent regulators of cellular signaling in response to different environmental stimuli and are mainly derived from superoxide anions (O_2^-), hydrogen peroxide (H_2O_2), and hydroxyl radicals (OH^-) (Mittal et al., 2014). It has been reported that ROS are involved in DNA repair, cell cycling, cell differentiation, chromatin remodeling, self-renewal, and other cell processes by Rendra et al. (Rendra et al., 2019). Furthermore, ROS plays an essential role in the regulation of macrophage polarization. A reduced ROS level suppresses the M1 phenotype and promotes macrophage polarization into the M2 phenotype (Zhou et al., 2018). However, the link between ROS and alloy-induced macrophage polarization has not been well-clarified.

Macrophages play a crucial role in the process of inflammation. Macrophages are able to secrete cytokines, chemokines, and growth factors to attract fibroblasts to produce extracellular matrix (ECM) and collagen. In addition, macrophages express different functional procedures by polarization according to different micro-environmental signals (McWhorter et al., 2015). Macrophages have two specific phenotypes, either M1-type macrophages (typically pro-inflammatory macrophages activated in response to Th1 cell–derived cytokines) or M2-type macrophages (anti-inflammatory macrophages activated in response to Th2 cell-derived cytokines) (Zhang et al., 2018).

In the process of 3D medical printing of titanium alloy, there may be partially melted or un-melted powder left on the surface of the material, which may lead to residual particle pollution in the later stage. Yi et al. (Yi et al., 2022) showed that acid etching treatment of porous Ti alloy scaffolds could remove residual powder on the surface of scaffolds and significantly improve the osteogenesis properties.

This study combines etched and unetched 3D printed Cu-bearing titanium with RAW 264.7 cells to explore the effect of macrophage biological behaviors, including the occurrence of an alloy being in direct contact with cells and alloy extracting culture macrophages. It could provide the experimental basis for animal and clinical use of this surface treatment technology.

2 Materials and methods

2.1 Material preparation

Plate samples with a size of 10 × 10 × 2 mm were fabricated by 3D printing technology. Selective laser melting (SLM) is one of the rapidly developed additive manufacturing techniques that creates solid models by adding powder layer by layer. The fabrication detail can be found in the previous studies (Zong et al., 2020); (Liu et al., 2021). According to a previous study, a Class 1 laser system equipped with a ProX DMP 200 fiber laser (a wavelength of 1070 nm and maximum output power of 300 W) was used to prepare Ti6Al4V-5Cu and Ti6Al4V-6Cu alloys (Zong et al., 2020). Laser power, scanning speed, scanning spacing, and single layer thickness are the major parameters

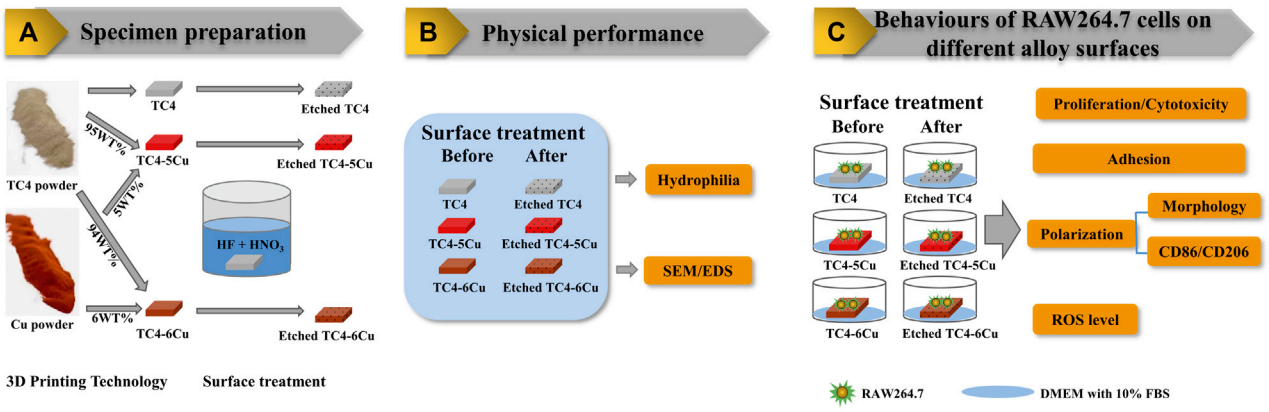

FIGURE 1
Flow diagram of the study: **(A)** Specimen preparation; **(B)** Physical performance; **(C)** Behaviours of RAW264.7 cells on different alloy surfaces.

in the process of selective laser melting. Different laser processing parameters were compared, and the optimal parameters were selected in this study: laser power of 260 W, scanning distance of 45 μm, and laser spot diameter of 70 μm. Then, all the samples were ground with waterproof SiC paper from 800 to 2000 grits. The specimens were subsequently immersed in nitric acid–hydrogen fluoride acid solution and finally washed with deionized water, acetone, and anhydrous ethanol for 10 min and dried by cold air. The ratio between nitric acid, fluoride acid, and distilled water is 1:4:5, and the etching duration is 30 s. The experimental samples were divided into six groups: unetched TC4 (TC4), unetched TC4-5Cu (TC4-5Cu), unetched TC4-6Cu (TC4-6Cu), etched TC4 (ETC4), etched TC4-5Cu (ETC4-5Cu), and etched TC4-6Cu (ETC4-6Cu). The preparation of the extract is according to ISO 10993–12 standards. Figure 1 illustrates the flow diagram of the study.

2.2 Surface characterization

2.2.1 Morphology

The structural morphology of the experimental samples was tested by using a scanning electron microscope (SEM, Zeiss Merlin Compact, Germany) equipped with energy-dispersive spectroscopy (EDS).

2.2.2 Hydrophilicity measurement

The surface wettability of the alloys was detected by the wettability measuring instrument (DataPhysics Instruments Gmbh, Germany) with the droplet method. The initial volume of the droplet is about 2 μl. SCA20 software was used to calculate the contact angles on the left and right sides of the samples. Three different areas were measured on each sample surface, and the process was repeated once.

2.3 Behaviors of RAW 264.7 cells on different material surfaces

2.3.1 Cell culture

Murine macrophage RAW 264.7 cells were used in this study. The cells were cultured in Dulbecco's modified Eagle's medium (DMEM, Hyclone, United States) supplemented with 10% FBS (Gibco) in an atmosphere of 5% CO_2 at 37°C. The cells were passaged at approximately 80% confluence and used at early passages (P5). The preparation of extracts included immersing the plate samples of etched and unetched titanium alloys in a cell culture medium for 72 h at a ratio of 0.2 g/ml according to ISO 10993–12 standard. After that, the extracts were collected, filtered by a 0.2-μm filter, and stored at 4°C.

2.3.2 Cell proliferation and cytotoxicity assay

RAW 264.7 cell proliferation was analyzed by the Cell Counting Kit-8 (CCK-8) for 12 and 24 h. RAW 264.7 cells were cultured at a concentration of 2×10^4 cells/ml and then seeded on all samples in a 96-well culture plate (500 μl/well, 37°C, 5% CO_2). The extract was changed the next day. After incubation for 12 and 24 h, respectively, the culture media was removed and 100 μl of DMEM medium with 10% CCK-8 (Beyotime, China) was added. Then, the samples were incubated in a dark incubator for 2 h at 37°C. Afterward, the 450 nm optical density (OD) was obtained with an Enzyme standard instrument (Multiskan GO, Thermo Scientific, United States). The cell relative growth rate (RGR) was calculated according to the following formula:

$$RGR = OD_{experimental\ group} / OD_{control\ group} \times 100\%.$$

2.3.3 Cell adhesion

RAW264.7 cells were seeded on different material surfaces at a concentration of 2×10^4 cell/ml for 24 h. After incubation, the medium was removed and the cells on alloys were washed three

times with phosphate-buffered saline (PBS) and fixed with 4% (w/v) paraformaldehyde for 10 min. And then, they were rinsed twice by PBS again and permeabilized with 0.2% (v/v) Triton X-100 (Beyotime, China) for 6 min. After that, 50 μL of rhodamine-phalloidin (Molecular, Probes Thermo Fisher Scientific, China) was added to stain cells in darkness. Finally, 5 mg/ml 40.6-diamidino-2-phenylindole (DAPI) solution was added to stain cells in darkness. The photographed stain images were observed by an optical microscope.

2.3.4 Cell morphology

RAW 264.7 cells were seeded in confocal dishes at a concentration of 2×10^4 cells/ml and cultured in different kinds of material extracts for 24 h. After incubation, the medium was removed and the cells were washed three times with phosphate-buffered saline (PBS) and fixed with 4% (w/v) paraformaldehyde for 10 min. Then, they were rinsed twice by PBS again and permeabilized with 0.2% (v/v) Triton X-100 (Beyotime, China) for 6 min. After that, 50 μl rhodamine–phalloidin (Molecular, Probes Thermo Fisher Scientific, China) was added to stain cells in darkness. Finally, 5 mg/ml Hoechst 33,342 (Boster, China) solution was added to stain cells in darkness. The photographed stain images were observed by a laser scanning confocal microscope.

2.3.5 Flow cytometry test

A total of 1×10^6 RAW 264.7 cells were collected and washed with PBS three times after being cultured in different material extracts for 12 and 24 h. APC-conjugated CD86 antibody (0.312 μg/test, Thermo Fisher Scientific) and PE-conjugated CD206 antibody (0.625 μg/test, Thermo Fisher Scientific) were incubated with the macrophages for 30 min on ice. Finally, PBS was added to the tubes to keep the final volume at 200–300 μL for flow cytometry (BD Pharmingen, San Diego, CA).

2.3.6 Measurement of intracellular reactive oxygen species

The intracellular ROS production was determined by a reactive oxygen species assay kit (Beyotime Biotechnology Ltd., Shanghai, China) for 12 and 24 h. RAW 264.7 cells were collected and incubated with DCFH-DA (1:1,000) for 30 min. The cells were washed twice with PBS, and fluorescence intensity was monitored by a flow cytometer (Becton Dickinson, America).

2.3.7 Statistical analysis

All experiments were analyzed with SPSS 23.0 software. The results are presented as mean ± standard deviation. Differences between groups were analyzed using one-way analysis of variance (ANOVA) followed by Tukey's test. p values less than 0.05 were considered statistically significant.

3 Result

3.1 Material preparation

A class 1 laser system equipped with a ProX DMP 200 fiber laser (a wavelength of 1070 nm and maximum output power of 300 W) was used to prepare Ti6Al4V-5Cu and Ti6Al4V-6Cu alloys, and the optimal parameters were selected in this study: laser power of 260W, scanning distance of 45 μm, and laser spot diameter of 70 μm (Zong et al., 2020).

According to ISO 10993–12 guidelines, the preparation of extracts included immersing the plate samples of etched and unetched titanium alloys in a cell culture medium for 72 h at a ratio of 0.2 g/ml. An analytical balance is used to measure the weight of each sample (Table 1). The average weight of the TC4 alloy, TC4-5Cu alloy, and TC4-6Cu alloy before etching and after etching are 0.0200g, 0.0236 g, and 0.0281 g, respectively, and there is no statistical difference ($p > 0.05$).

3.2 Characterizations of alloy

3.2.1 Surface morphology

Figure 2 shows the microstructures of the TC4 alloy surface, TC4-5Cu alloy surface, and TC4-6Cu alloy surface before and after acid etching technology. From the macro-graph of material samples (Figure 2A), the surface of each alloy sample after grinding and polishing is relatively smooth. SEM analysis reveals that the surface of TC4 alloy (Figures 2A,B), TC4-5Cu alloy (Figure 2B), and TC4-6Cu alloy (Figures 2B,C) is flat and smooth, while the surface of ETC4 alloy (Figure 2B–A'), ETC4-5Cu alloy (Figure 2B–B'), and ETC4-6Cu alloy (Figure 2B–C') was characterized by micro-porous structures. Most of the visible elements in the present alloys are titanium (Ti) and a small amount of aluminum (AI) and vanadium (V). Meanwhile, copper (Cu) can be detected in TC4-5Cu alloy (as shown in Figures 2B,C) and TC4-6Cu alloy (as shown in Figure 2C).

3.2.2 Hydrophilicity

As shown in Figure 3, the contact angle of TC4, TC4-5Cu, and TC4-6Cu groups and ETC4, ETC4-5Cu, and ETC4-6Cu groups are 72.14 ± 4.081, 63.23 ± 8.321, and 67.81 ± 3.763 and 68.95 ± 8.536, 64.3 ± 3.972, and 71.07 ± 3.854, respectively. The contact angle of TC4-5Cu and ETC4-5Cu groups is smaller than that of the others, but had no statistical significance ($p > 0.05$).

3.3 Behaviors of RAW 264.7 cells on different material surfaces

3.3.1 Cell proliferation and cytotoxicity

Figure 4A shows the optical densities of RAW 264.7 cells in different alloy extracts. With the increase in incubation time, there is a significant increase in OD values in each group, indicating the number of RAW 264.7 cells in each alloy

TABLE 1 Weight of the samples.

Sample	Before etching (g)	After etching (g)	Weight loss (g)	Average weight loss (g)
TC4	0.8347	0.8152	0.0195	0.0200
	0.8343	0.8103	0.0240	
	0.8354	0.8116	0.0238	
	0.8351	0.8213	0.0138	
TC4-5Cu	0.6280	0.6156	0.0124	0.0236
	0.6258	0.6155	0.0103	
	0.6248	0.5942	0.0306	
	0.6153	0.5743	0.041	
TC4-6Cu	0.8908	0.8797	0.0111	0.0281
	0.8874	0.8574	0.0300	
	0.8861	0.8546	0.0315	
	0.8847	0.8449	0.0398	

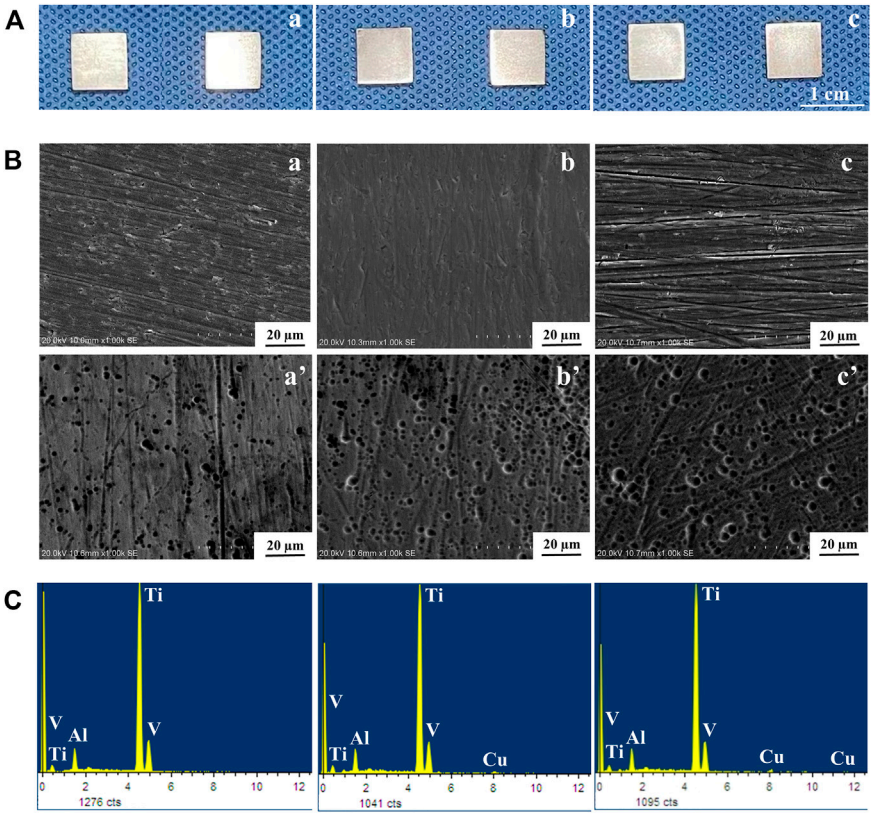

FIGURE 2
Surface morphology of alloys: **(A)** macro images of alloys; **(B)** SEM images of alloys; **(C)** EDS analyses of alloys: **(A)** TC4 alloy and **(a')** ETC4 alloy; **(B)** TC4-5Cu alloy and **(b')** ETC4-5Cu alloy; **(C)** TC4-6Cu alloy and **(c')** ETC4-6Cu alloy.

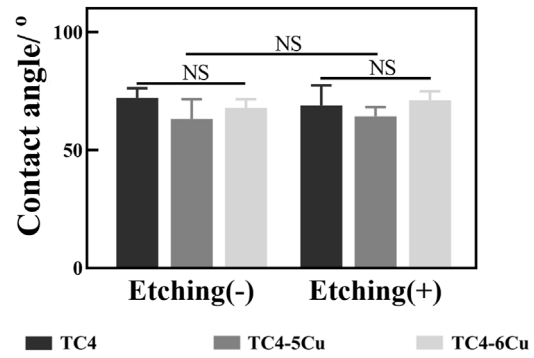

FIGURE 3
Contact angle of samples (n = 10, NS: No significant difference).

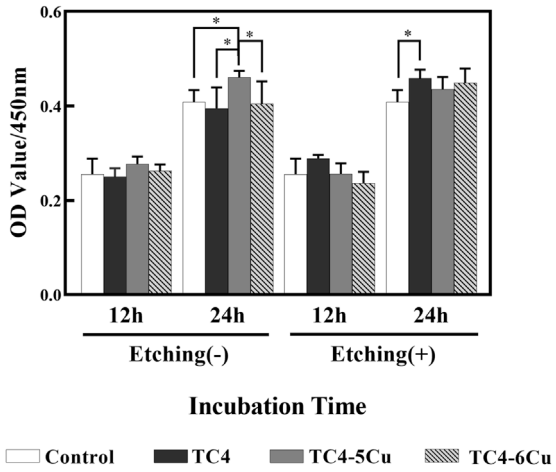

FIGURE 4
Cell proliferation of RAW 264.7 cells cultured in different alloy extracts for 12 and 24 h (n = 5, *p < 0.05)

extract increased. At the time of 12h, there is no difference between groups among unetched alloy groups. At the time of 24 h, the absorbance of the TC4-5Cu group is significantly higher than that of other groups ($p < 0.05$) among unetched groups; the absorbance of the ETC4 group is higher than that of the control group ($p < 0.05$). The relative growth rates (RGR) of RAW 264.7 cells in different alloy extracts are shown in Table 2. The cell toxicity grade (CTG) is obtained according to the standard United States Pharmacopeia. From 12 to 24 h of incubation, all the experimental groups show grades 0 to 1 (no toxicity).

3.3.2 Cell adhesion

Figure 5A shows the adhesion of RAW 264.7 macrophages cultured on different alloy samples for 24 h. Red fluorescence represents F-actin, and blue fluorescence represents the nucleus. Compared with the TC4-5Cu group, the numbers of RAW 264.7 cells in TC4-6Cu are higher. It could be seen that compared with all unetched groups and the ETC4 group, the numbers of RAW 264.7 cells in ETC4-5Cu and ETC4-6Cu groups are higher, and the areas of the red stained cytoskeleton of RAW 264.7 cells are also larger, that indicated that the morphology of RAW 264.7 cells is also more extended (Figure 5A).

TABLE 2 Relative growth rate (RGR) and cytotoxicity level at different detection periods.

		12 h		24 h	
		RGR	grade	RGR	grade
Before etching	TC4	97.96 ± 7.17	1	96.66 ± 10.90	1
	TC4-5Cu	108.70 ± 6.04	0	112.69 ± 3.36	0
	TC4-6Cu	102.77 ± 5.40	0	98.99 ± 11.65	0
After etching	TC4	113.13 ± 3.11	0	112.26 ± 4.41	1
	TC4-5Cu	100.40 ± 8.66	0	106.55 ± 6.32	1
	TC4-6Cu	92.72 ± 9.32	1	109.89 ± 7.47	1

3.3.3 Cell morphology

The morphology of RAW 264.7 cells cultured in all alloy extracts for 24 h is shown in Figure 6A. Red fluorescence stands for F-actin, and blue fluorescence represents the nucleus. The unactivated M0 phenotype macrophages are spherical-like. M1 phenotype macrophages are characterized by rounded-like shapes with extended spread area, while macrophages with M2 phenotype are usually elongated. After 24 h of inoculation, RAW 264.7 cells in extracts of all alloy samples expand pseudopodia and connect, while the cells incubated in different exact alloy samples show different morphology. Most RAW 264.7 cells are activated in etched groups, showing M1 or M2 phenotype, and generally showing elongated spindle shape with an obvious extension of filamentous pseudopodia. However, in unetched groups, RAW 264.7 macrophages show round structure in almost all alloy extracts except TC4-6Cu alloy. The extension of RAW 264.7 cells is more obvious in the ETC4-5Cu and ETC4-6Cu groups than in the ETC4 group (Figure 6A).

3.3.4 M1/M2 phenotype of macrophages

Figure 7A,B shows the expression of M1-type marker CD86 and M2-type marker CD206 in RAW 264.7 cells cultured on the surface of different alloy samples for 12 and 24 h. After 12 h culture (Figure 7A), the expression of CD86 in TC4 alloy, TC4-5Cu alloy, and TC4-6Cu alloy increased by 2.26%, 2.54%, and 4.73%, respectively, and the expression of

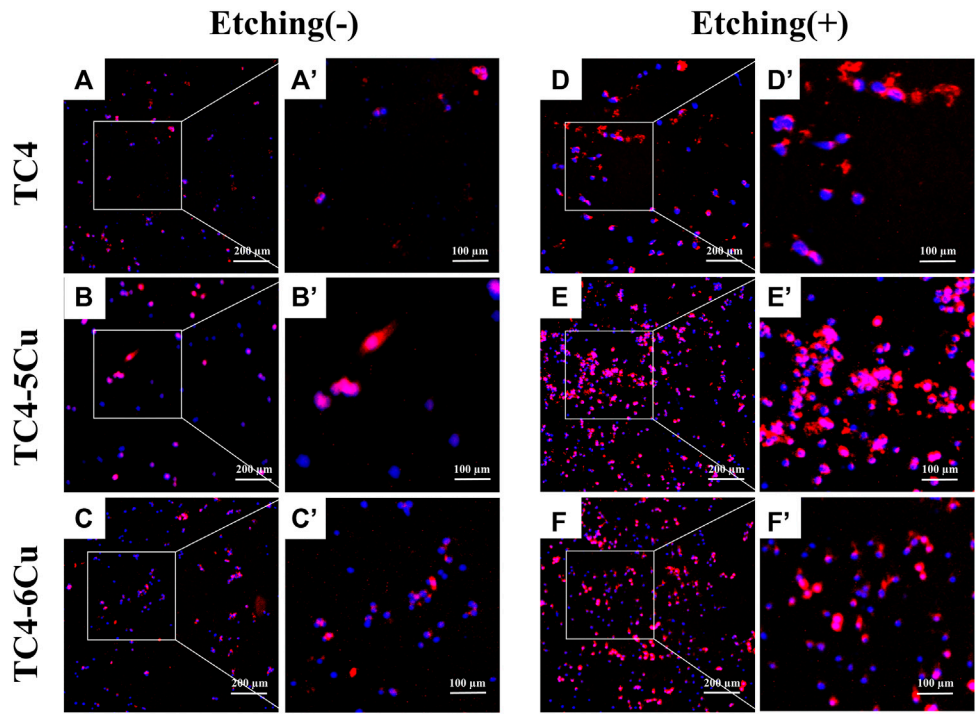

FIGURE 5
Cell adhesion of RAW 264.7 cells cultured on the surface of different alloys for 24 h. **(a′–f′)** is a partial enlargement of the selected area of **(A–F)**.

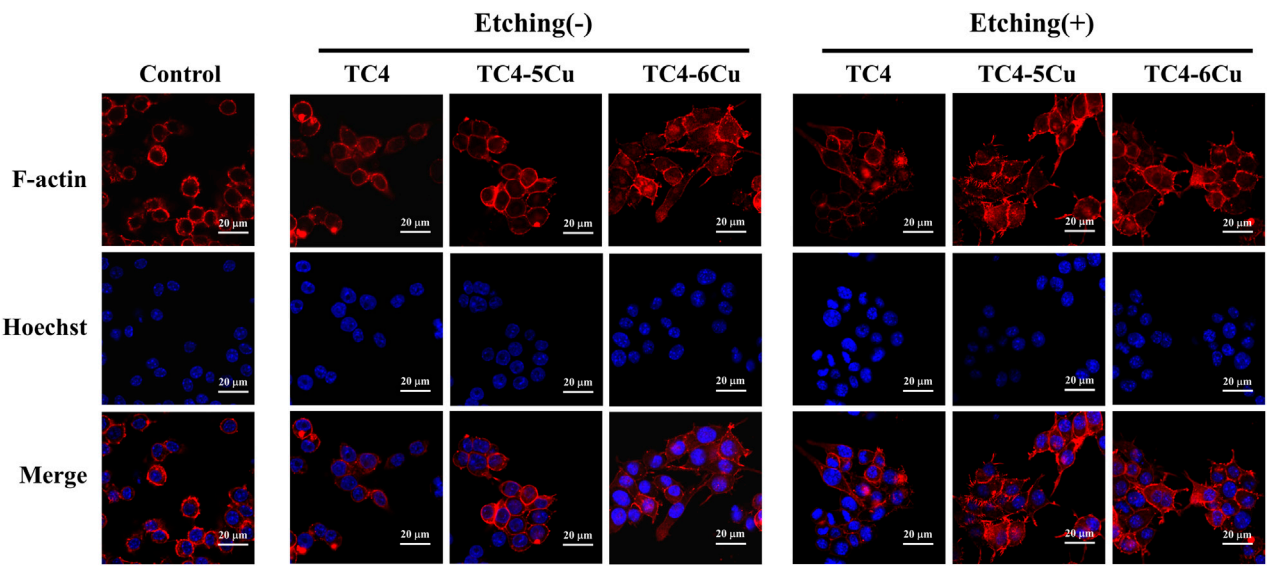

FIGURE 6
Morphology of RAW 264.7 cells cultured in different alloy extracts for 24 h.

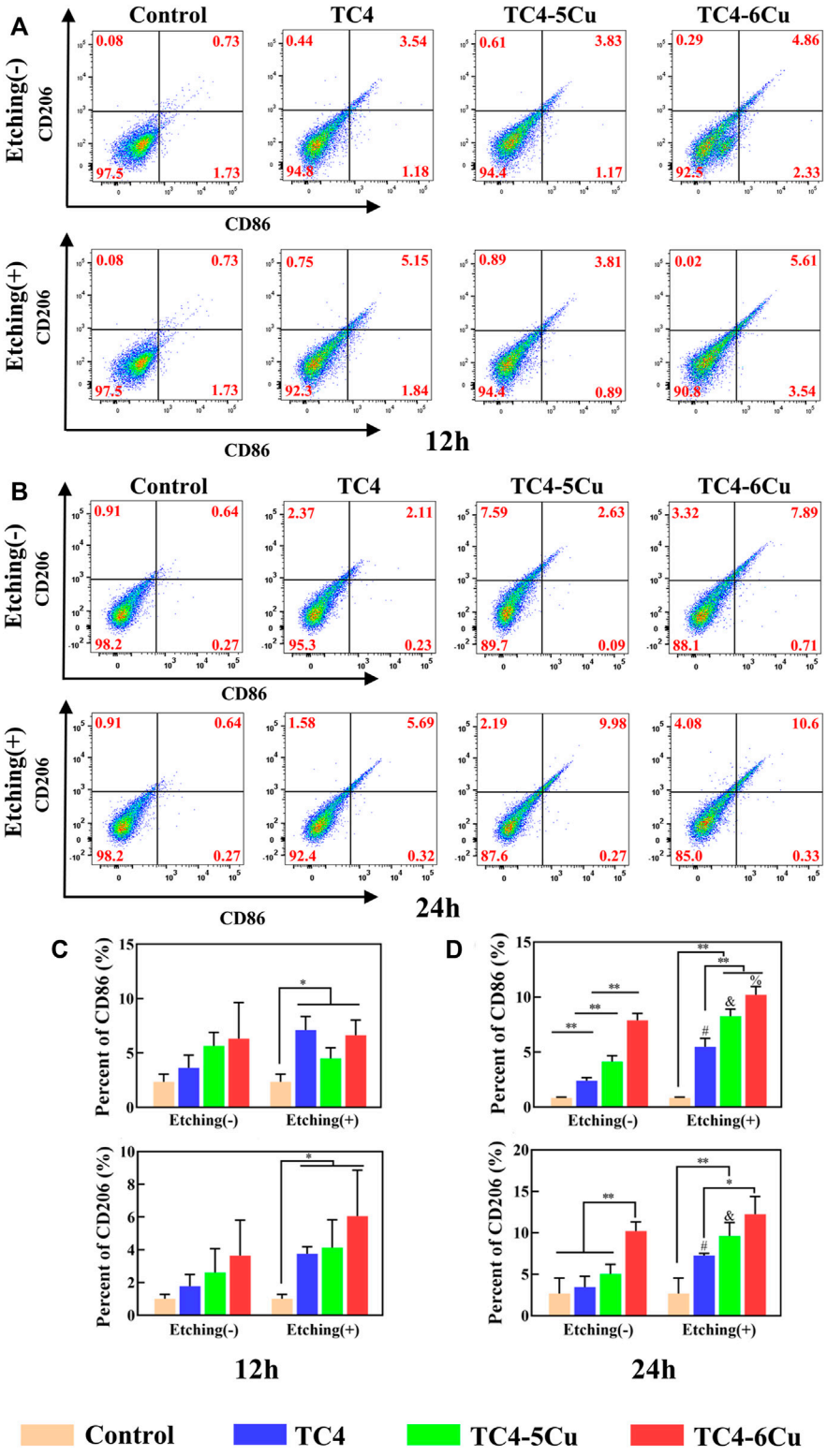

FIGURE 7
Flow cytometry analysis of RAW 264.7 cell surface markers cultured in different alloy extracts for 12 and 24 h **(A,C)** Expression of CD86 and CD206 in different alloy extracts for 12 h; **(B,D)** expression of CD86 and CD206 in different alloy extracts for 24 h (NS: No significant difference; *$p < 0.05$; **$p < 0.01$; #, compared with TC4 alloy, $p < 0.05$; and, compared with TC4-5Cu alloy, $p < 0.05$; %, compared with TC4-6Cu alloy, $p < 0.05$)

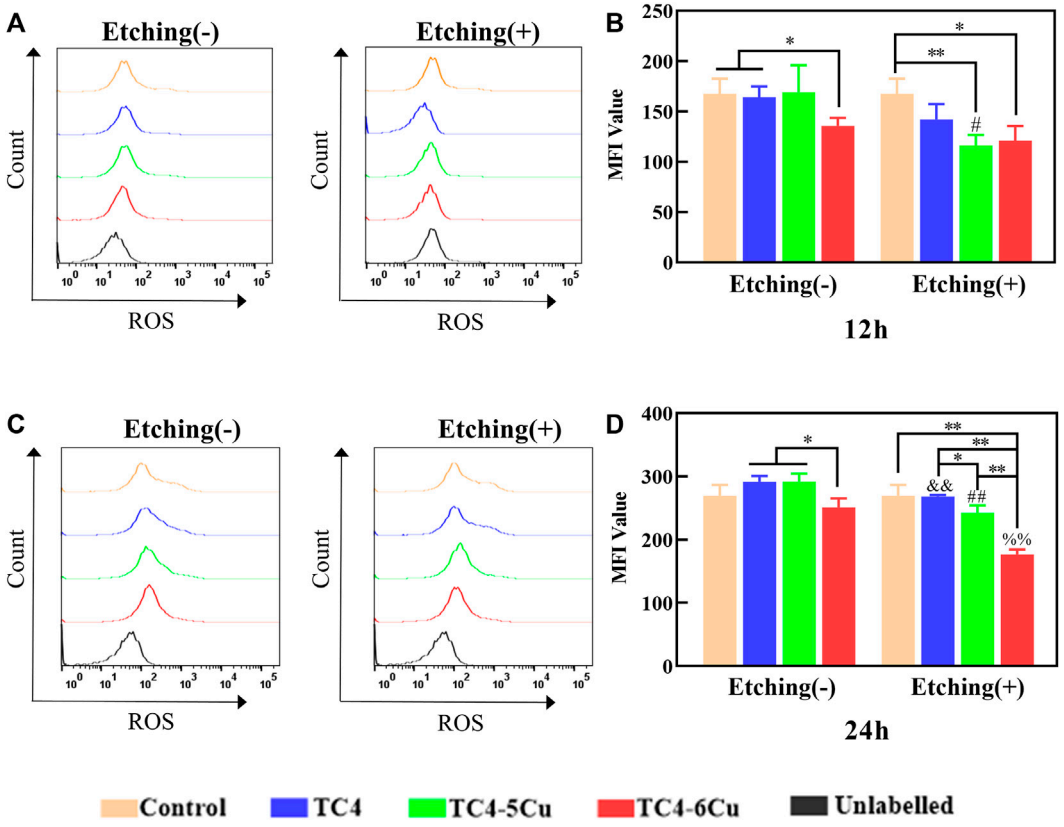

FIGURE 8
Flow cytometry analysis of intracellular ROS levels on RAW 264.7 cells in different material extracts for 12 and 24 h. **(A,C)** Expression of ROS in different alloy groups for 12 and 24 h; **(B,D)** quantification of mean fluorescence intensity (MFI) of intracellular ROS level in different alloy groups for 12 and 24 h (n = 3, NS: No significant difference; *$p < 0.05$; **$p < 0.01$; and, compared with TC4 alloy, $p < 0.01$; ##, compared with TC4-5Cu alloy, $p < 0.01$; %%, compared with TC4-6Cu alloys, $p < 0.01$)

CD206 increased by 3.17%, 3.63%, and 4.34% compared with the control group, respectively. The CD86 marker of ETC4 alloy, ETC4-5Cu alloy, and ETC4-6Cu alloy increased by 4.53%, 2.24%, and 6.69%, respectively, and the CD206 marker of ETC4 alloy, ETC4-5Cu alloy, and ETC4-6Cu alloy increased by 5.09%, 3.89%, and 4.82% compared with the control group, respectively. After 24 h of culture (Figure 7B), the expression of CD86 in TC4 alloy, TC4-5Cu alloy, and TC4-6Cu alloy increased by 1.43%, 1.81%, and 7.69%, and the expression of CD206 increased by 2.93%, 8.67%, and 9.66% compared with the control group, respectively. The expression of CD86 of ETC4 alloy, ETC4-5Cu alloy, and ETC4-6Cu alloy increased by 5.1%, 9.34%, and 10.02%, and the expression of CD206 of ETC4 alloy, ETC4-5Cu alloy, and ETC4-6Cu alloy increased by 5.72%, 10.62%, and 13.13% compared with the control group, respectively.

Statistical analysis results display that after 12 h of culture (Figure 7C), there is no significant difference in CD86 and CD206 expression between unetched alloy groups and the control group, but the expression levels of CD86 and CD206 of etched alloy groups are significantly higher than those of the control group ($p < 0.05$). After 24 h (Figure 7D), the expression levels of CD86 and CD206 in the ETC4, ETC4-5Cu, and ETC4-6Cu groups increase compare to the TC4, TC4-5Cu and TC4-6Cu groups ($p < 0.05$), indicating that acid etching could increase the expression of CD86 and CD206. The expression of CD86 in the TC4-6Cu, TC4-5Cu, and TC4 group decreases gradually ($p < 0.05$), and the expression of CD206 in the TC4-6Cu group is significantly higher than that of the TC4 group ($p < 0.05$), indicating that Cu-bearing titanium alloy could increase the expression of CD86 and CD206. The expression of CD86 of ETC4-5Cu and ETC4-6Cu groups is significantly higher than that of the ETC4 group ($p < 0.01$), and the expression of CD206 of ETC4-6Cu alloy is significantly higher than that of ETC4 alloy ($p < 0.05$).

3.3.5 Intracellular reactive oxygen species level

Flow cytometry is used to detect the ROS expression of RAW 264.7 cells cultured in different alloy sample extracts for 12 and 24 h (Figure 8). After 12 h, the ROS level in ETC4-5Cu is significantly lower than that of the TC4-5Cu group ($p < 0.05$).

The ROS level of TC4-6Cu alloy is significantly lower than that of the control group and TC4 group ($p < 0.01$); the ROS levels of ETC4-5Cu alloy ($p < 0.01$) and ETC4-6Cu alloy ($p < 0.05$) are significantly lower than those of the control group. After 24 h, the ROS level in etched groups is significantly lower than that of unetched groups ($p < 0.01$). The ROS level of TC4-6Cu alloy is significantly lower than that of TC4 alloy and TC4-5Cu alloy ($p < 0.05$); the ROS level of the ETC4-6Cu group is significantly lower than that of other etched groups ($p < 0.01$), and the ROS level of ETC4-5Cu alloy is significantly lower than that of ETC4 alloy ($p < 0.05$).

4 Discussion

The 3D printing technology used in this study is selective laser melting (SLM), which creates solid models by adding powder layer by layer. Laser power, scanning speed, scanning spacing, and single layer thickness are the major parameters in the process of selective laser melting. Different laser processing parameters were compared, and the optimal parameters were selected in this study: laser power of 260 W, scanning distance of 45 μm, and laser spot diameter of 70 μm. Physical and chemical characteristics of implant material surfaces, such as surface morphology and hydrophilicity, can play a crucial role in the process of bone integration (Smeets et al., 2016). Copper, as an essential trace mineral for human beings, has been proven to have excellent antibacterial properties and has been widely used in titanium alloy–related studies (Fan et al., 2022). In this study, TC4-5Cu alloy and TC4-6Cu alloy were made by adding different content of copper into TC4 alloy using 3D printing technology, and the printed alloys were treated by a traditional acid etching technique.

The ratio of HF, HNO_3, and H_2O used in acid etching treatment and the acid etching duration all affect the surface morphology of TC4 alloy, and the etching duration is particularly important. It is reported that hydrophilic surfaces with lower contact angles are more conducive to cell attachment and proliferation (Rupp et al., 2017). It was found that the hydrophilicity was not significantly affected by acid etching (Figure 3). Therefore, the differences in cell growth and attachment between groups were not related to their hydrophilicity. In addition to hydrophilicity, the release of metal ions may also affect cell proliferation and adhesion (Lai et al., 2020). Acid etching may generate increased immersion of copper ions that could affect cell proliferation and adhesion. In a previous study, it was shown that etched TC4 alloy surface in HF-HNO3 solution may lead to selective dissolution of α-phase and selective enrichment of β-phase on the alloy surface (Sittig et al., 1999). In addition, acid etching treatment could also clean pollution particles on the surface of TC4 alloy (Yi et al., 2022).

This study prepared alloy extracts from TC4, TC4-5Cu, and TC4-6Cu alloys ETC4, ETC4-5Cu, and ETC4-6Cu alloys according to ISO10993-12. The copper element in the alloy was gradually dissolved and released into the medium, thus affecting the biological behavior of macrophages in the material alloy extracts. However, high doses of copper can lead to formation of free radicals and induce cytotoxicity by causing chromosome and DNA damage (Sharma et al., 2021). In this study, the CCK-8 test showed that Cu-bearing titanium alloys (TC4-5Cu alloy and TC4-6Cu alloy) had no effect on the viability of RAW 264.7 cells compared with the TC4 alloy, and all Cu-bearing TC4 alloy samples had no cytotoxicity (Figure 4). Therefore, Cu-bearing titanium alloys could be used as long-term implantation materials. In addition, acid etching treatment did not affect the cell viability of various alloys and proven to have no cytotoxicity.

In this study, the adhesion of RAW 264.7 cells on the surface of alloy materials was observed by staining. The results showed that RAW 264.7 cells could attach and extend well on the surface of all alloy samples after 24 h incubation (Figure 5). Meanwhile, compared with the surface of the TC4 alloy, the surface of Cu-bearing titanium alloys (TC4-5Cu alloy and TC4-6Cu alloy) is beneficial for the adhesion of RAW 264.7 macrophages (Figure 5). The surface of TC4-6Cu alloy shows better cell adhesion ability than that of TC4-5Cu alloy. The possible reasons are as follows: 1) with the increase of copper content, the porosity of TC4 alloy also increases, and the surface area of Cu-bearing titanium alloy and cells also increases correspondingly, which improves the ability of cell adhesion; 2) Protein adsorption is the prerequisite for cell adhesion to biomaterials (Yang et al., 2021), and the hydrophilic surface of Cu-bearing titanium alloy may promote protein adsorption. The possible reasons are as follows: 1) with the increase of copper content, the porosity of TC4 alloy also increases, and the surface area of Cu-bearing titanium alloy and cells also increases correspondingly, which improves the ability of cell adhesion; 2) protein adsorption is the prerequisite for cell adhesion to biomaterials (Yang et al., 2021), and the hydrophilic surface of Cu-bearing titanium alloy may promote protein adsorption. The etched alloy samples showed stronger cell adhesion to RAW 264.7 cells than that of unetched alloy samples (Figure 5). The reasons may be as follows: 1) acid etching treatment improves the surface morphology of the alloy, and micro-porous structures, which were observed by SEM (Figure 2B), could increase the surface area of material alloys and immerse more copper ions to promote cell adhesion; 2) acid etching treatment can clean the pollution particles on the surface of TC4 alloy, which is more conducive to the growth of cells.

Confocal microscopy was used to observe the cell morphology of RAW 264.7 cells in different alloy extracts. Macrophages can polarize into different phenotypes to perform different functions. The shapes of polarized macrophages are different. M1-type macrophages are generally “fried egg-shaped” and M2-type macrophages were mostly long spindle-shaped (McWhorter et al., 2013). In this study, the RAW

264.7 cells cultured in etched sample extracts for 24 h are activated and show the structural features of the M2 phenotype, including elongated spindle shape and filamentous pseudopodia; while the cell structures of unetched groups are mostly round. (Figure 6). In addition, RAW 264.7 cells in etched Cu-bearing titanium alloy groups (ETC4-5Cu alloy and ETC4-6Cu alloy) have more obvious filamentous pseudopod extension and interconnection. (Figure 6).

The observed macrophage surface marker proteins were detected by flow cytometry in different groups. The results showed that the expression of M1-type surface marker CD86 and M2-type surface marker CD206 was increased in Cu-bearing titanium alloy groups, indicating that copper in Cu-containing titanium alloys could promote the polarization of macrophages. Compared with the same alloy before and after acid etching, CD86 and CD206 in etched groups were significantly higher than those in unetched groups, indicating that etching treatment could promote the polarization of macrophages (Figure 7).

The production of reactive oxygen species (ROS) is the core of inflammatory response in the early implantation stage. Oxidative stress occurs when ROS levels exceed the antioxidant defenses in cells, leading to irreversible intracellular damage (Schieber and Chandel, 2014). In the production process of 3D printed medical titanium alloy, partially melted or un-melted powder may remain on the surface of the materials and may lead to residual particle pollution and ROS generation in the adhesion cells. In this study, RAW 264.7 cells were cultured in the alloy sample extracts to detect the ROS production level. The results showed that at the time of 24 h, ROS levels in all etched alloy groups were significantly reduced compared with those in unetched alloy groups (Figure 8). The possible reason is that the acid etching treatment cleans the residual particles on the surface of the alloy. The ROS level in ETC4-5Cu and ETC4-6Cu alloy groups is obviously lower than that of other groups. The ROS level in the TC4-6Cu alloy group is lower than that of TC4-5Cu, and the ROS level in the ETC4-6Cu alloy group is lower than that of the ETC4-5Cu alloy group. With the increase in copper content, the ROS levels decreased. These results suggest that ROS production may be closely related to phenotype switching of macrophages, and ROS production may promote the M1-type macrophage polarization.

Macrophages are considered to be one of the earliest cells reaching the surface of the implant. The appropriate inflammatory reaction between the macrophage and implant is beneficial for the success of implantation (Franz et al., 2011). Macrophages polarize into M1 type (classical activation type) or M2 type (alternative activation type), expressing different functional programs according to different micro-environmental signals (Linares et al., 2016). M1 macrophages mainly exist in the early stage of inflammation and act as pro-inflammatory cells to spread the inflammatory response to downstream immune cells. M2 macrophages mainly contribute to stopping inflammation and promoting tissue repair and wound healing. It was reported that M1-type macrophages are dominant in the failed tissues surrounding implants, while M2-type macrophages are dominant in the normal tissues surrounding implants by Tazzyman et al. (Tazzyman et al., 2013). In this study, the etched alloy surfaces with lower ROS levels could promote macrophages to polarize to the M2-type phenotype, thus contributing to the increase in the success rate of implant implantation. This may be caused by acid etching treatment which makes the surface of the material form a microporous structure and more copper-element can be precipitated from the copper-bearing titanium alloy. The copper element can activate macrophages and tends to polarize macrophages to M2-phenotype.

However, the polarization of macrophages on different Cu-bearing alloy surfaces is not only closely related to ROS levels but also affected by the levels of many inflammatory factors. Therefore, the relevant inflammatory factors on RNA and protein levels need further exploration in the following experiments.

5 Conclusion

All samples had no toxicity to RAW 264.7 cells. With the increase of copper content, the adhesion ability of cells on the surface of the material was enhanced. Adding copper to TC4 alloys could activate the polarization of macrophages on the surface of TC4 alloy and reduce the ROS level. Surface treatment by acid etching had no effect on the hydrophilicity of the alloy surface. Acid etching treatment also could enhance cell adhesion, activate macrophage polarization, and reduce ROS levels. The *in vitro* experiments of this study indicated that acid-etched 3D printed copper-bearing titanium alloy could promote the adhesion and polarization of macrophages and provide a promising implant material for the treatment of peri-implant inflammation.

Data availability statement

The original contributions presented in the study are included in the article/Supplementary Material; further inquiries can be directed to the corresponding authors.

Author contributions

BL and HK contributed to the conception and design of the study. QW designed and prepared the materials. JY performed

the experiments and wrote the manuscript. HK helped perform the analysis with constructive discussion. WH polished the language of the article. All authors have read and approved the final version of the manuscript.

Funding

This study was financially supported by the Natural Science Foundation Project of Liaoning Province (Nos. 2020-MS-150 and 2018225059) and Guangxi Key Laboratory of the Rehabilitation and Reconstruction for Oral and Maxillofacial Research Funded Project (No. GXKLRROM2107).

Conflict of interest

The authors declare that the research was conducted in the absence of any commercial or financial relationships that could be construed as a potential conflict of interest.

Publisher's note

References

Carter, S.-S. D., Costa, P. F., Vaquette, C., Ivanovski, S., Hutmacher, D. W., Malda, J., et al. (2017). Additive biomanufacturing: an advanced approach for periodontal tissue regeneration. *Ann. Biomed. Eng.* 45 (1), 12–22. doi:10.1007/s10439-016-1687-2

Chen, X., Li, H. S., Yin, Y., Feng, Y., and Tan, X. W. (2015). Macrophage proinflammatory response to the titanium alloy equipment in dental implantation. *Genet. Mol. Res.* 14 (3), 9155–9162. doi:10.4238/2015.August.7.25

Dawood, A., Marti, B. M., Sauret-Jackson, V., and Darwood, A. (2015). 3D printing in dentistry. *Br. Dent. J.* 219 (11), 521–529. doi:10.1038/sj.bdj.2015.914

Fan, D.-Y., Yi, Z., Feng, X., Tian, W.-Z., Xu, D.-K., Cristino Valentino, A. M., et al. (2022). Antibacterial property of a gradient Cu-bearing titanium alloy by laser additive manufacturing. *Rare Met.* 41 (2), 580–593. doi:10.1007/s12598-021-01826-w

Franz, S., Rammelt, S., Scharnweber, D., and Simon, J. C. (2011). Immune responses to implants - a review of the implications for the design of immunomodulatory biomaterials. *Biomaterials* 32 (28), 6692–6709. doi:10.1016/j.biomaterials.2011.05.078

Huang, Q., Ouyang, Z., Tan, Y., Wu, H., and Liu, Y. (2019). Activating macrophages for enhanced osteogenic and bactericidal performance by Cu ion release from micro/nano-topographical coating on a titanium substrate. *Acta Biomater.* 100, 415–426. doi:10.1016/j.actbio.2019.09.030

Javaid, M., and Haleem, A. (2019). Current status and applications of additive manufacturing in dentistry: a literature-based review. *J. oral Biol. craniofacial Res.* 9 (3), 179–185. doi:10.1016/j.jobcr.2019.04.004

Lai, Y., Xu, Z., Chen, J., Zhou, R., and Cai, Y. (2020). Biofunctionalization of microgroove surfaces with antibacterial nanocoatings. *BioMed Res. Int.* 2020, 1–13. doi:10.1155/2020/8387574

Linares, J., Fernandez, A. B., Feito, M. J., Matesanz, M. C., Sanchez-Salcedo, S., Arcos, D., et al. (2016). Effects of nanocrystalline hydroxyapatites on macrophage polarization. *J. Mat. Chem. B* 4 (11), 1951–1959. doi:10.1039/c6tb00014b

Liu, Z., Liu, Y., Liu, S., Wang, D., Yi, Z., Sun, L., et al. (2021). The effects of TiO_2 nanotubes on the biocompatibility of 3D printed Cu-bearing TC4 alloy. *Mater. Des.* 207 (20), 109831. doi:10.1016/j.matdes.2021.109831

McWhorter, F. Y., Davis, C. T., and Liu, W. F. (2015). Physical and mechanical regulation of macrophage phenotype and function. *Cell. Mol. Life Sci.* 72 (7), 1303–1316. doi:10.1007/s00018-014-1796-8

McWhorter, F. Y., Wang, T., Phoebe, N., Thanh, C., and Liu, W. F. (2013). Modulation of macrophage phenotype by cell shape. *Proc. Natl. Acad. Sci. U. S. A.* 110 (43), 17253–17258. doi:10.1073/pnas.1308887110

Mittal, M., Siddiqui, M. R., Tran, K., Reddy, S. P., and Malik, A. B. (2014). Reactive oxygen species in inflammation and tissue injury. *Antioxidants Redox Signal.* 20 (7), 1126–1167. doi:10.1089/ars.2012.5149

Olivares-Navarrete, R., Hyzy, S. L., Slosar, P. J., Schneider, J. M., Schwartz, Z., Boyan, B. D., et al. (2015). Implant materials generate different peri-implant inflammatory factors. *Spine* 40 (6), 399–404. doi:10.1097/brs.0000000000000778

Palaskar, J., Nadgir, D. V., and Shah, I. (2010). Effect of recasting of nickel: chromium alloy on its castability. *J. Indian Prosthodont. Soc.* 10 (3), 160–164. doi:10.1007/s13191-010-0033-x

Rendra, E., Riabov, V., Mossel, D. M., Sevastyanova, T., Harmsen, M. C., Kzhyshkowska, J., et al. (2019). Reactive oxygen species (ROS) in macrophage activation and function in diabetes. *Immunobiology* 224 (2), 242–253. doi:10.1016/j.imbio.2018.11.010

Rupp, F., Liang, L., Geis-Gerstorfer, J., Scheideler, L., and Hüttig, F. (2017). Surface characteristics of dental implants: a review. *Dent. Mater. official Publ. Acad. Dent. Mater.* 34. doi:10.1016/j.dental.2017.09.007

Schieber, M., and Chandel, N. S. (2014). ROS function in redox signaling and oxidative stress. *Curr. Biol.* 24 (10), R453–R462. doi:10.1016/j.cub.2014.03.034

Sharma, P., Goyal, D., Baranwal, M., and Chudasama, B. (2021). Oxidative stress induced cytotoxicity of colloidal copper nanoparticles on RAW 264.7 macrophage cell line. *J. Nanosci. Nanotechnol.* 21 (10), 5066–5074. doi:10.1166/jnn.2021.19365

Sittig, C., Textor, M., Spencer, N. D., Wieland, M., and Vallotton, P. H. (1999). Surface characterization of implant materials c.p. Ti, Ti-6Al-7Nb and Ti-6Al-4V with different pretreatments. *J. Mat. Sci. Mat. Med.* 10 (1), 35–46. doi:10.1023/a:1008840026907

Smeets, R., Stadlinger, B., Schwarz, F., Beck-Broichsitter, B., Jung, O., Precht, C., et al. (2016). Impact of dental implant surface modifications on osseointegration. *Biomed Res. Int.* 2016, 6285620. doi:10.1155/2016/6285620

Spriano, S., Yamaguchi, S., Baino, F., and Ferraris, S. (2018). A critical review of multifunctional titanium surfaces: new frontiers for improving osseointegration and host response, avoiding bacteria contamination. *Acta Biomater.* 79, 1–22. doi:10.1016/j.actbio.2018.08.013

Sun, Y., Li, Y., Wu, B., Wang, J., Lu, X., Qu, S., et al. (2017). Biological responses to M13 bacteriophage modified titanium surfaces *in vitro*. *Acta Biomater.* 58, 527–538. doi:10.1016/j.actbio.2017.06.019

Tazzyman, S., Niaz, H., and Murdoch, C. (2013). Neutrophil-mediated tumour angiogenesis: subversion of immune responses to promote tumour growth. *Seminars Cancer Biol.* 23 (3), 149–158. doi:10.1016/j.semcancer.2013.02.003

Yang, J., Qin, H., Chai, Y., Zhang, P., Chen, Y., Yang, K., et al. (2021). Molecular mechanisms of osteogenesis and antibacterial activity of Cu-bearing Ti alloy in a bone defect model with infection *in vivo*. *J. Orthop. Transl.* 27, 77–89. doi:10.1016/j.jot.2020.10.004

Yi, Z., Liu, Y., Ma, Y., Liu, Z., Sun, H., Zhou, X., et al. (2022). Surface treatment of 3D printed Cu-bearing Ti alloy scaffolds for application in tissue engineering. *Mater. Des.* 213, 110350. doi:10.1016/j.matdes.2021.110350

Zhang, B., Liu, Y., Lan, X., Xu, X., Zhang, X., Li, X., et al. (2018). Oral *Escherichia coli* expressing IL-35 meliorates experimental colitis in mice. *J. Transl. Med.* 16, 71. doi:10.1186/s12967-018-1441-7

Zhang, E., Ren, J., Li, S., Yang, L., and Qin, G. (2016). Optimization of mechanical properties, biocorrosion properties and antibacterial properties of as-cast Ti-Cu alloys. *Biomed. Mat.* 11 (6), 065001. doi:10.1088/1748-6041/11/6/065001

Zhou, Y., Que, K. T., Zhang, Z., Yi, Z. J., Zhao, P. X., You, Y., et al. (2018). Iron overloaded polarizes macrophage to proinflammation phenotype through ROS/acetyl-p53 pathway. *Cancer Med.* 7 (8), 4012–4022. doi:10.1002/cam4.1670

Zong, W., Zhang, S., Zhang, C., Ren, L., and Wang, Q. (2020). Design and characterization of selective laser-melted Ti6Al4V–5Cu alloy for dental implants. *Mater. Corros.* 71, 1697. doi:10.1002/maco.202011650